JOURNAL OF GEOPHYSICAL RESEARCH, VOL. 93, NO. D8, PAGES 9405-9417, AUGUST 20, 1988

Rossby Wave Activity in a Two-Dimensional Model: Closure for Wave Driving and Meridional Eddy Diffusivity

MATTHEW H. HITCHMAN[1]

National Center for Atmospheric Research, Boulder, Colorado

GUY BRASSEUR

Belgian Institute for Space Aeronomy, Brussels, Belgium

A parameterization of the effects of Rossby waves in the middle atmosphere is proposed for use in two-dimensional models. By adding an equation for conservation of Rossby wave activity, closure is obtained for the meridional eddy fluxes and body force due to Rossby waves. Rossby wave activity is produced in a climatological fashion at the tropopause, is advected by a group velocity which is determined solely by model zonal winds, and is absorbed where it converges. Absorption of Rossby wave activity causes both an easterly torque and an irreversible mixing of potential vorticity, represented by the meridional eddy diffusivity, K_{yy}. The distribution of Rossby wave driving determines the distribution of K_{yy}, which is applied to all of the chemical constituents. This provides a self-consistent coupling of the wave activity with the winds, tracer distributions, and the radiative field. Typical winter stratospheric values for K_{yy} of 2×10^6 m^2 s^{-1} are obtained. Poleward tracer advection is enhanced and meridional tracer gradients are reduced where Rossby wave activity is absorbed in the model.

1. INTRODUCTION

Two-dimensional models are being used extensively in attempts to understand a variety of phenomena, including the effect of trace gases on the distributions of ozone and temperature. The chief advantage over one-dimensional photochemical models is their ability to represent the effects of dynamics in redistributing constituents in the latitude-height plane. In the middle atmosphere, mean meridional circulations and irreversible mixing are caused primarily by wave absorption. The eddies which are responsible for these zonal mean dynamical effects are either small-scale (gravity waves) or fundamentally three-dimensional (Rossby waves). Only zonal mean variables are calculated in two-dimensional models. Yet eddy flux convergence terms appear in the zonal mean equations. This presents a closure problem. In the real atmosphere, gravity wave and Rossby wave absorption will vary with latitude, altitude, and time, in accordance with variations in wave generation and, primarily, variations in background winds. Thus it is highly desirable to capture the interactive nature of the waves and zonal mean flow in a two-dimensional model through a reasonable parameterization.

All closure methods require the use of auxilliary information. One strategy is simply to specify a meridional circulation and constant eddy mixing coefficients. Since the zonal mean equations are coupled, it is desirable at least to have self-consistent meridional circulations and eddy mixing coefficients. For self-consistency, eddy forcing and heating rates must be calculated from the same data or the same model variables. Mixing coefficients may be derived from three-dimensional general circulation model (GCM) calculations [*Kida*, 1983; *Plumb and Mahlman*, 1987], or from Lagrangian models employing satellite-derived winds [*Lyjak*, 1987], and subsequently used in a two-dimensional model. However, the mean state of a two-dimensional model may be rather different than that of a GCM or of the real world at a particular time, making it difficult to maintain self-consistency. For Rossby waves, observations have been used in a climatological specification of the meridional eddy diffusivity, K_{yy} [*Newman et al.*, 1986, 1988]. *Jackman et al.* [1988] employed observationally based K_{yy}s and meridional circulations estimated from the same data to obtain self-consistent estimates of N_2O distributions in their two-dimensional model. *Gray and Pyle* [1987] have studied the equatorial stratopause semiannual oscillation with a two-dimensional model, wherein Rossby wave driving is specified climatologically and its effects on the mean meridional circulation are included. A different self-consistent approach was devised by *Tung* [1987] which requires only observed temperatures and ozone as input. Heating rates are calculated, yielding the meridional circulation. The zonal mean equations are solved for the distribution of wave driving, which then gives the distributions of K_{yy}.

The two-dimensional models of *Garcia and Solomon* [1985], *Gray and Pyle* [1987], and *Brasseur and Hitchman* [1987] include the important effects of gravity wave breaking. They make use of the *Lindzen* [1981] and *Holton* [1982] parameterization, which provides the gravity wave driving contribution to the meridional circulation and a determination of the vertical eddy diffusivity, K_{zz}. Here we propose a method, based on the principle of conservation of wave activity, which allows an interactive determination of the effects of Rossby waves in the presence of an evolving background state.

Schoeberl and Strobel [1978] made an early closure attempt for stationary Rossby waves by solving a separate

[1] Now at Department of Meteorology, University of Wisconsin-Madison.

Paper number 8D0179.
0148-0227/88/008D-0179$05.00

planetary wave structure equation for geopotential, similar to that studied for a fixed basic state by *Schoeberl and Geller* [1977]. Unfortunately, the wave-mean flow scheme did not converge for typical observed wave amplitudes. The wave activity equation we have added to our model is simple and couples readily into the transformed Eulerian zonal mean equations. The auxilliary information required for closure is removed one step: a damping profile and a climatological source of Rossby wave activity must be specified.

Our two-dimensional model, which is briefly described in section 2, is formulated in transformed Eulerian coordinates, similar to the model of *Garcia and Solomon* [1983]. This allows a straightforward interpretation of the effects of waves on the mean circulation. Several physical processes are hidden in assuming that fluxes can be represented by mixing coefficients and mean gradients. In section 2 we clarify what we intend to represent by K_{yy} and outline the method of deriving K_{yy} from model variables. In section 3 we describe the conservation equation for Rossby wave activity and the relations which determine wave driving and eddy mixing based on wave activity flux convergence. Certain simplifying assumptions enable a group velocity to be calculated which depends solely on model zonal winds and latitude. Following a discussion of the numerical algorithm and the propagation properties of wave activity in the model, diagrams of wave activity, wave driving, and meridional diffusivity are presented in section 4. The primary purpose of this paper is to describe the parameterization and underlying theory. Some initial results regarding the impact of this parameterization on model dynamics and tracer distributions are presented in section 5.

2. Theoretical Background

2.1 The BISA/NCAR Model

This radiative-chemical-dynamical model was designed at the Belgian Institute for Space Aeronomy (BISA) and further developed at the National Center for Atmospheric Research (NCAR). The model extends from 85°S to 85°N and the surface to 85 km, with a grid spacing of 5° in latitude and 1 km in altitude. As in the work by *Garcia and Solomon* [1983], entropy and chemical species are advected by a residual (transformed Eulerian) mean meridional circulation in log-pressure coordinates, which is forced by spatial gradients in wave driving and radiative heating or cooling. The zonal mean thermodynamic energy, zonal momentum, mass continuity, and thermal wind equations are

$$\frac{\partial \bar{\theta}}{\partial t} + \bar{v}^* \frac{\partial \bar{\theta}}{\partial y} + \bar{w}^* \frac{\partial \bar{\theta}}{\partial z} = \bar{Q} + D_\theta \tag{1}$$

$$\frac{\partial \bar{u}}{\partial t} - \eta\ \bar{v}^* + \frac{\partial \bar{u}}{\partial z}\ \bar{w}^* = \Sigma F \tag{2}$$

$$\frac{1}{\cos\phi}\frac{\partial}{\partial y}\left(\cos\phi\ \bar{v}^*\right) + \frac{1}{\rho_o}\frac{\partial}{\partial z}\left(\rho_o\ \bar{w}^*\right) = 0 \tag{3}$$

$$\eta\ \frac{\partial \bar{u}}{\partial z} \approx -\ \frac{g}{\bar{\theta}}\ \frac{\partial \bar{\theta}}{\partial y} \tag{4}$$

where the absolute vorticity is

$$\eta = f - \frac{1}{\cos\phi}\frac{\partial}{\partial y}(\cos\phi\ \bar{u})$$

$$\eta = f + 2\ \bar{u}\ \frac{\tan\phi}{a}$$

and the eddy flux terms are

$$D_\theta = -\frac{1}{\rho_o}\frac{\partial}{\partial z}\left[\rho_o\left(\overline{w'\theta'} + \frac{\bar{\theta}_y}{\bar{\theta}_z}\ \overline{v'\theta'}\right)\right] \tag{5}$$

$$\Sigma F = F_R + F_g + F_K + F_t + F_i + F_m \tag{6}$$

Variables are defined in the notation list. For the purposes of this study, we ignore the effects of Kelvin waves, tides, ion drag, and molecular diffusion. Wave driving by Rossby and gravity waves is given by the divergence of wave activity flux:

$$F_R + F_g = \frac{1}{\rho_o\ a\ \cos\phi}\ \vec{\nabla}\cdot\vec{F} \tag{7}$$

where

$$F_y = \rho_o\ a\ \cos\phi\left[\frac{\bar{u}_z}{\bar{\theta}_z}\ \overline{v'\theta'} - \overline{u'v'}\right] \tag{8a}$$

$$F_z = \rho_o\ a\ \cos\phi\left[\frac{\eta}{\bar{\theta}_z}\ \overline{v'\theta'} - \overline{u'w'}\right] \tag{8b}$$

In (5) and (8) gravity wave driving primarily involves vertical fluxes, while Rossby wave driving is primarily identifiable with meridional fluxes. In the quasi-geostrophic version of (8), applicable to extratropical Rossby waves, the terms involving $\bar{u}_z$ and w' are ignored, and $\eta = f$.

The zonal wind equation (2) is not solved explicitly in the model. Instead, the strategy is to determine the residual circulation, to integrate the temperature equation in time, then to calculate new zonal winds via the thermal wind equation (4). Equations (1)-(4) can be combined to give a diagnostic equation for the residual mean meridional stream function:

$$C_{zz}\frac{\partial^2\chi}{\partial z^2} + C_z\frac{\partial\chi}{\partial z} + C_{yz}\frac{\partial^2\chi}{\partial y\partial z}$$

$$+C_y\frac{\partial\chi}{\partial y} + C_{yy}\frac{\partial^2\chi}{\partial y^2} = \cos\phi\ C_F \tag{9}$$

where the coefficients on the left-hand side of (9) are functions of $\bar{u}$ and $\bar{\theta}$, the circulation is related to the stream function by

$$\bar{v}^* = -\frac{1}{\cos\phi}\frac{1}{\rho_o}\frac{\partial}{\partial z}(\rho_o\chi) \tag{10a}$$

$$\bar{w}^* = \frac{1}{\cos\phi}\frac{\partial\chi}{\partial y} \tag{10b}$$

and the forcing term is

$$C_F = \frac{R}{H}\frac{\partial}{\partial y}(\bar{Q} - D_\theta) + f\frac{\partial}{\partial z}(\Sigma F) \tag{11}$$

[*Garcia and Solomon*, 1983]. Given the forcing term, previous values of $\bar{T}$ and $\bar{u}$, and the boundary conditions $\chi = 0$ at the poles ($\bar{v}^* = 0$), $\partial\chi/\partial z = 0$ at the top,

and a specified lower boundary condition, the meridional circulation is obtained. Then the distributions of potential temperature and chemical constituents are updated from (1) and

$$\frac{\partial \overline{\mu}}{\partial t} + \overline{v}^* \frac{\partial \overline{\mu}}{\partial y} + \overline{w}^* \frac{\partial \overline{\mu}}{\partial z} = S_\mu + D_\mu \tag{12}$$

where μ is the mass mixing ratio of a particular tracer, and the eddy flux convergence terms are

$$D_\mu = -\frac{1}{\rho_o}\frac{\partial}{\partial z}\left[\rho_o \ \overline{w'\mu'}\right] - \frac{1}{\cos\phi}\frac{\partial}{\partial y}\left[\cos\phi \ \ \overline{v'\mu'}\right]$$

$$-\frac{1}{\rho_o}\frac{\partial}{\partial z}\left[\rho_o \ \frac{\overline{v'\theta'}}{\overline{\theta}_z}\right]\overline{\mu}_y + \frac{1}{\cos\phi}\frac{\partial}{\partial y}\left[\cos\phi \ \ \frac{\overline{v'\theta'}}{\overline{\theta}_z}\right]\overline{\mu}_z \tag{13}$$

Equations (1) and (12) are solved with an implicit time integration scheme, using an alternating direction method [*Carnahan et al.*, 1969]. We use a 15-day time step, which allows for inexpensive multiyear integrations.

Note that the transformation

$$\overline{v} = \overline{v}^* + \frac{1}{\rho_o}\frac{\partial}{\partial z}\left[\rho_o \ \frac{\overline{v'\theta'}}{\overline{\theta}_z}\right] \tag{14a}$$

$$\overline{w} = \overline{w}^* - \frac{1}{\cos\phi}\frac{\partial}{\partial y}\left[\cos\phi \ \ \frac{\overline{v'\theta'}}{\overline{\theta}_z}\right] \tag{14b}$$

is asymmetric with respect to eddy velocity: only v' appears. With this transformation, potential temperature is affected only by vertical gradients of eddy fluxes (5). The second two terms in D_μ (13) arise from this transformation, a minor complication which is offset by the conceptual simplicity of regarding $\overline{v}^*$, hence meridional advection, as being directly proportional to wave driving. D_θ is generally small, except in the mesosphere, where gravity wave breaking leads to a significant downward heat flux [*Coy and Fritts*, 1988].

To close (1)-(4) and (12) we need Q, F_R, F_g, $\overline{v'\theta'}$, $\overline{w'\theta'}$, $\overline{v'\mu'}$, and $\overline{w'\mu'}$. Q may be calculated in two ways: fast or accurate. For the purposes of this study, we use the fast algorithm. IR transfer is approximated by a Newtonian relaxation toward a seasonally varying climatological temperature cross section, while the parameterization of *Schoeberl and Strobel* [1978] is used for insolation absorption by ozone. In the next section we describe how the eddy fluxes are represented in terms of eddy diffusivities and mean gradients. The breaking gravity wave parameterization of *Lindzen* [1981] and *Holton* [1982] is used, together with model zonal winds to determine the distribution of wave driving, F_g, and vertical eddy diffusivity, K_{zz}, due to gravity waves. A description of this parameterization and its effects in the BISA/NCAR model is given by *Brasseur and Hitchman* [1987]. An anologous parameterization of F_R and K_{yy}, wave driving and meridional eddy diffusivity due to Rossby waves, is proposed in section 3.

2.2 Mixing Length Theory

A common method for treating the eddy fluxes in (5) and (13) is to parameterise them in terms of background gradients and mixing coefficients. Although linear mixing length theory has clear limitations, it can shed light on the physical mechanisms involved. Some of the following ideas are also discussed by *Garcia and Solomon* [1983] and *Smith et al.* [1988]. Turbulent mixing, photochemical effects, and wave growth and decay can each give rise to a tracer flux. For clarity, we consider the meridional flux alone. Figure 1 shows a situation where $\overline{\mu}$ increases northward linearly. In the presence of a wave, parcels will oscillate meridionally. Consider a parcel of air, smaller than the scale of wave variation, which is in equilibrium with its environment: $\mu' = 0$. If it is displaced northward, in the absence of dissipation it will move along path 1. The value of μ in the parcel will not change, but relative to its zonal mean environment, $\mu' = -\eta' \ \overline{\mu}_y$, where η' is the meridional displacement. If wave amplitudes are too large, parcels will range across a region where the variation in $\overline{\mu}$ is not simply linear and this representation for μ' is no longer valid. The use of diffusion coefficients derived from linear mixing length theory is strictly valid only for small-amplitude waves.

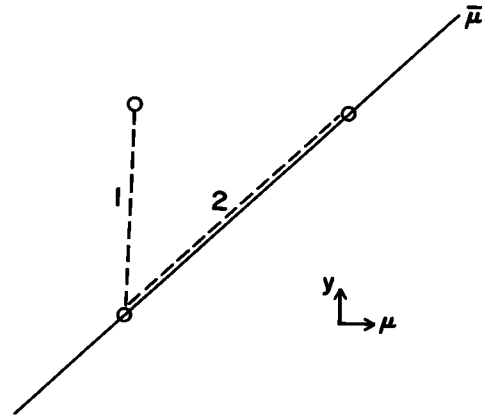

Fig. 1. Schematic diagram of a northward parcel excursion across a tracer gradient in the presence of a planetary Rossby wave. Along path 1 the parcel mixing ratio does not change. Along path 2 the parcel equilibrates completely to local values and loses its identity. In either limit there is no net flux. A flux occurs for any intermediate path, where advection and mixing have comparable time scales.

Photochemical processes are likely to cause a parcel to become more like its environment, so that a northward displaced parcel will lie between paths 1 and 2. This would also be the case for parcel dilution by turbulent mixing. The linearized eddy tracer equation for horizontal motions is

$$\frac{\partial \mu'}{\partial t} + \overline{u}\frac{\partial \mu'}{\partial x} + v'\frac{\partial \overline{\mu}}{\partial y} = -\frac{\mu'}{\tau_m} - \frac{\mu'}{\tau_\mu} \tag{15}$$

where τ_m is a mechanical mixing time scale arising from turbulence and is considered to apply to all constituents equally, and τ_μ is a relaxation time scale arising from air parcels traveling through an environment with varying photochemical equilibrium values and is specific to the particular constituent. For plane waves that can propagate or change amplitude, μ', $\eta' \sim \exp i\theta$, where $\theta = k(x - ct)$ and $c = c_r + ic_i$. With this assumption, $\partial/\partial t + \overline{u}(\partial/\partial x) \rightarrow i/\tau_a + 1/\tau_g$, where τ_a is an advective time scale and τ_g is a wave growth time scale. Equation (15) then becomes

$$\mu'\left[\frac{1}{\tau_m}+\frac{1}{\tau_\mu}+\frac{1}{\tau_q}+\frac{i}{\tau_a}\right]=-\left[\frac{1}{\tau_q}+\frac{i}{\tau_a}\right]\quad \eta'\quad \bar{\mu}_y \qquad (16)$$

The complex conjugate of v' is $v'^* = [(1/\tau_q + i/\tau_a)\eta']^* = (1/\tau_q - i/\tau_a)\eta'^*$. Since $\overline{\eta'\eta'^*} = |\eta'|^2 \equiv \eta_o^2$ and $\overline{v'\mu'} = \frac{1}{2}\overline{Re[v'^*\mu']}$,

$$\overline{v'\mu'} = -\frac{\left[1/\tau_a^2+1/\tau_q^2\right]\left[1/\tau_m+1/\tau_\mu+1/\tau_q\right]}{\left[(1/\tau_m+1/\tau_\mu+1/\tau_q)^2+1/\tau_a^2\right]}\quad \frac{1}{2}\eta_o^2\quad \bar{\mu}_y \qquad (17)$$

The flux will be zero, unless there are parcel displacements across a background gradient ($\frac{1}{2}\eta_o^2 \quad \bar{\mu}_y \neq 0$). The coefficient of $\bar{\mu}_y$ in (17) may be regarded as a mixing coefficient: K^μ_{yy}. An eddy flux divergence thus takes the form of diffusion of the zonal mean quantity. Three limits are now examined for the time scales in (17).

1. For steady waves ($\tau_q \to \infty$) and no photochemical effect ($\tau_\mu \to \infty$),

$$\overline{v'\mu'} = -\frac{\tau_m}{\tau_a^2+\tau_m^2}\quad \frac{1}{2}\eta_o^2\quad \bar{\mu}_y \qquad (18)$$

The coefficient of $\bar{\mu}_y$ in (18) is a neutral mixing coefficient, which applies to all tracers. This results from mixing of air down to very small scales. In the absence of turbulence ($\tau_m \to \infty$) or in the presence of very fast turbulence ($\tau_m \ll \tau_a$), $\overline{v'\mu'} = 0$, and there is no flux. With no turbulence an air parcel maintains its original property, moving along path 1 through a wave (Figure 1). No exchange with the environment occurs, so there is no flux. With extremely rapid mixing, a parcel will lose its identity before getting very far, moving along path 2. With $\mu' = 0$ always, there can be no flux. It can easily be shown that the neutral mixing coefficient, hence the downgradient flux, is largest when $\tau_a = \tau_m$.

2. For steady waves and no turbulent mixing, (18) is obtained, but with τ_μ replacing τ_m. The coefficient of $\bar{\mu}_y$ in this case accounts for a redistribution of tracer $\bar{\mu}$ via photochemical effects. It is not applicable to other tracers, unless they have similar photochemical properties. For potential vorticity, τ_μ is a radiative decay time scale. It is possible to have a flux of potential vorticity associated with radiative damping, and zero flux for an inert constituent. If $\tau_\mu = \infty$, parcels do not relax to their new environment and move along path 1; there is no flux. If $\tau_\mu = 0$, parcels equilibrate to their local environment so rapidly that $\mu' = 0$ always (path 2), and there is no flux. But if $\tau_\mu \sim \tau_a$, there can be a net flux due to parcels traveling through a varying photochemical regime, even with no turbulent parcel dispersion or wave growth. This is the so-called photochemical eddy transport.

3. In the absence of turbulence or photochemical effects (τ_m, $\tau_\mu \to \infty$), wave activity entering or leaving a region can cause a temporary flux:

$$\overline{v'\mu'} = -\frac{1}{\tau_q}\quad \frac{1}{2}\eta_o^2\quad \bar{\mu}_y \qquad (19)$$

During wave growth ($\tau_q > 0$) the flux is downgradient. During wave decay ($\tau_q < 0$) the flux is upgradient. Integrated over the transit time of a wave packet through a region there is no net flux.

We are interested in estimating tracer fluxes for time scales longer than the temporal envelope of a wave event, hence hereafter consider only the case where $\tau_q = \infty$. For quasi-geostrophic Rossby waves the meridional flux of eddy potential vorticity is proportional to the divergence of quasi-geostrophic Eliassen-Palm flux, or EP flux:

$$\overline{v'q'} = \frac{1}{\rho_o\ a\ cos\phi}\vec{\nabla}\cdot\vec{F}_q \qquad (20)$$

[*Edmon et al.*, 1980]. On the time scale of a month, $\vec{\nabla}\cdot\vec{F}_q \approx 0$, unless there is mechanical or radiative damping. Consider (17) as applying to q', with $\tau_q = \infty$, and define a mixing coefficient for q':

$$\overline{v'q'} = -K^q_{yy}\quad \bar{q}_y \qquad (21)$$

[e.g., *Newman et al.*, 1986], where

$$K^q_{yy} = \frac{(1/\tau_m+1/\tau_q)}{1+(\tau_a/\tau_m+\tau_a/\tau_q)^2}\quad \frac{1}{2}\eta_o^2 \qquad (22)$$

and τ_q is the radiative relaxation time relevant to q'. Combining (20) and (21),

$$K^q_{yy} = -\frac{\vec{\nabla}\cdot\vec{F}_q}{\rho_o\ a\ cos\ \phi\ \ \bar{q}_y} \qquad (23)$$

The dissipative processes responsible for Rossby wave driving are also responsible for irreversible mixing of potential vorticity. If $\vec{\nabla}\cdot\vec{F}_q$ can be determined from a conservation equation for wave activity, then K^q_{yy} is known.

If $\tau_\mu \approx \tau_q$ for a particular tracer then K^q_{yy} can be used in (12) for that tracer. In a Rossby wave surf zone, τ_m is small, so that limit 1 obtains, and $K^\mu_{yy} \approx K^q_{yy}$. For $\tau_m \gg \tau_q, \tau_\mu$, limit 2 obtains, and a ratio can be formed:

$$K^\mu_{yy} = K^q_{yy}\quad \frac{\tau_\mu}{\tau_q}\quad \frac{\tau_a^2+\tau_q^2}{\tau_a^2+\tau_\mu^2} \qquad (24)$$

K^μ_{yy} and K^q_{yy} will both be small in the situation where advective and relaxation time scales are not similar, by previous reasoning, so differences between them will not be important. If $\tau_a \sim \tau_q$, then

$$K^\mu_{yy} = K^q_{yy}\quad \frac{2\tau_\mu\tau_q}{\tau_q^2+\tau_\mu^2} \qquad (25)$$

If τ_μ differs from τ_q by less than a factor of 2, then $K^\mu_{yy} \approx K^q_{yy}$. In this paper we assume that K^q_{yy} and K_{zz} apply to all tracers equally. For some constituents this may not be a good approximation.

In seeking to represent entropy and tracer flux convergences in the latitude-height plane by diffusion, it is convenient if we can assume that the ellipticity of air parcel trajectories is small. This leads to a conceptual simplicity in which vertical mixing is interpreted as being due to gravity waves and meridional mixing to Rossby waves. Although parcel trajectories through Rossby waves are elliptical [*Wallace*, 1978], *Jackman et al.* [1988] present evidence which suggests that terms involving $\overline{w'\eta'}$ and $\overline{v'\zeta'}$ contribute less than 10% to fluxes of N_2O in a two-dimensional model. See *Smith et al.* [1988] for a discussion of the relative importance of these K_{yz} terms for other tracers. If we assume that $\overline{w'\eta'} \approx 0 \approx \overline{v'\zeta'}$, then $\overline{v'\mu'} \approx -K_{yy}\ \bar{\mu}_y$ and $\overline{w'\mu'} \approx -K_{zz}\ \bar{\mu}_z$. In that case, (5)

and (13) simplify to

$$D_\theta \approx \frac{1}{\rho_o}\frac{\partial}{\partial z}\left[\rho_o\left(K_{zz}+\left(\frac{\overline{\theta}_y}{\overline{\theta}_z}\right)^2 K_{yy}\right)\overline{\theta}_z\right] \tag{26}$$

and

$$D_\mu \approx \frac{1}{\rho_o}\frac{\partial}{\partial z}\left[\rho_o\ K_{zz}\ \overline{\mu}_z\right]+\frac{1}{cos\phi}\frac{\partial}{\partial y}\left[cos\phi\ K_{yy}\ \overline{\mu}_y\right]$$

$$+\frac{1}{\rho_o}\frac{\partial}{\partial z}\left[\rho_o\ K_{yy}\ \frac{\overline{\theta}_y}{\overline{\theta}_z}\right]\overline{\mu}_y-\frac{1}{cos\ \phi}\frac{\partial}{\partial y}\left[cos\ \phi\ K_{yy}\ \frac{\overline{\theta}_y}{\overline{\theta}_z}\right]\overline{\mu}_z \tag{27}$$

Since Rossby wave motions are primarily meridional, whereas gravity waves have a very limited meridional extent, we make the simplifying, but compatible, assumption that in (26) and (27) K_{zz} is due entirely to gravity wave absorption and K_{yy} is due entirely to Rossby wave absorption.

3. Rossby Wave Activity and Group Velocity

Rossby wave activity is conserved unless there is wave generation or dissipation:

$$\frac{\partial A}{\partial t}+\vec{\nabla}\cdot\vec{F}=D \tag{28}$$

[*Edmon et al.*, 1980]. Equation (28) is the generalized Eliassen-Palm relation, in which $\vec{F}$ represents the transport of wave activity. A group velocity for Rossby waves can be defined if wave amplitude, zonal wind, density, and dissipation are assumed to vary much more slowly in space and time than the phase of an individual wave. In this slowly varying theory, or WKBJ approximation, $\vec{F}=\vec{G}A$. One choice for the definition of Rossby wave activity,

$$A=\frac{1}{2}\ \rho_o\ a\ \overline{q}_y\ \eta_o^2 \tag{29}$$

has units of kg m^{-1} s^{-1}, which allows the relationship to the Eliassen-Palm flux components (8) to be dimensionally correct:

$$F_y=G_yA,\qquad F_z=G_zA,$$

$$\vec{\nabla}\cdot\vec{F}=\frac{1}{cos\ \phi}\frac{\partial}{\partial y}\left(cos\ \phi\ G_yA\right)+\frac{\partial}{\partial z}\left(G_zA\right) \tag{30}$$

Andrews [1987] gives a detailed discussion of the various forms of A. If we can determine $\vec{\nabla}\cdot\vec{F}$ and D, then the solution to (28) provides F_R for use in (9). If $\vec{F}$ is assumed to be quasi-geostrophic, then K_{yy}^q is known through (23). D will be described in section 4. Linear quasi-geostrophic theory provides an expression for $\vec{G}$. The remainder of this section deals with the determination of $\vec{G}$.

We seek a representation of the group velocity which captures the essential physics of wave activity propagation on a sphere but depends only on $\overline{u}(y, z)$ and latitude. It is interesting to compare the group velocity derived for plane waves on a mid latitude beta-plane with that on a sphere. It can be shown that for undamped quasi-geostrophic planetary waves on a beta-plane, the dispersion relation is

$$\omega=\overline{u}\ k-\frac{k}{K^2}\ \overline{q}_y \tag{31a}$$

where

$$K^2=k^2+l^2+\frac{f_o^2}{N^2}\left(m^2+\frac{1}{4H^2}\right) \tag{31b}$$

and

$$\overline{q}_y=\beta-\overline{u}_{yy}-\frac{1}{\rho_o}\frac{\partial}{\partial z}\left(\rho_o\frac{f^2}{N^2}\frac{\partial\overline{u}}{\partial z}\right) \tag{31c}$$

[*Holton*, 1980]. In (31), $f_o=2\Omega sin\ \phi_o$, $\beta=(2\Omega/a)cos\phi_o$, and $k=k^*/(a\ cos\ \phi_o)$ = constant, while l and m are expected to vary with $\overline{u}$ and $\overline{q_y}$. The group speeds are

$$G_y=\frac{\partial\omega}{\partial l}=\frac{2lk^*}{a\ cos\ \phi_o\ K^4}\quad\overline{q}_y \tag{32a}$$

$$G_z=\frac{\partial\omega}{\partial m}=\frac{2mk^*}{a\ cos\ \phi_o\ K^4}\quad\overline{q}_y\quad\frac{f_o^2}{N^2} \tag{32b}$$

When Rossby wave activity extends over a broad range in latitude, these relations are less valid. In particular, k should not be independent of latitude on a sphere for a discrete value of k^*.

On the sphere, $f=2\ \Omega\ sin\ \phi$, $\beta=(2\Omega/a)\ cos\ \phi$, $k=k^*/(a\ cos\ \phi)$, and the dispersion relation is

$$\omega=\frac{\overline{u}\ s}{a\ cos\ \phi}-\frac{s}{a\ cos\ \phi\ L^2}\quad\overline{q}_y \tag{33a}$$

where

$$L^2=\frac{n(n+1)}{a^2}+\frac{f^2}{N^2}\left(m^2+\frac{1}{4H^2}\right) \tag{33b}$$

[*Haurwitz*, 1940]. Although n actually takes on discrete values, relations analogous to (32) for the sphere may be defined from (33a):

$$\frac{\partial\omega}{\partial n}=\frac{(2n+1)s}{a\ cos\ \phi\ L^4}\quad\overline{q}_y \tag{34a}$$

$$\frac{\partial\omega}{\partial m}=\frac{2ms}{a\ cos\ \phi\ L^4}\quad\overline{q}_y\quad\frac{f^2}{N^2} \tag{34b}$$

In comparing (31) with (33) and (32) with (34), the main difference for the sphere is simply $\phi\neq$ constant. This supports the strategy of examining the propagation of plane waves on the sphere [e.g., *Butchart et al.*, 1982]. For calculations on the sphere, it is appropriate to retain the dependence of f on $sin\ \phi$, of β on $cos\ \phi$, and of the zonal wave scale on $cos\ \phi$ for the group velocity. It is known from observations that G_z/G_y decreases toward the equator as a result of decreasing f [e.g., *Hitchman et al.*, 1987]. *Hoskins et al.* [1977] discuss the importance of retaining the latitudinal dependence of β when studying energy propagation on a sphere. Hereafter, we use the formulae derived for the beta-plane, (31) and (32), but allow ϕ to vary.

Equation (31) describes the basic structure of a Rossby wave. In addition, the meridional and vertical wave

numbers for each zonal wave number can change following the group velocity through shear. This allows for the possibility of poleward refraction. Remembering that $\omega = \omega(l, m, y, z)$, the conservation of wave crests relations can be derived:

$$\frac{dl}{dt} = -k \frac{\partial \bar{u}}{\partial y} \tag{35a}$$

$$\frac{dm}{dt} = -k \frac{\partial \bar{u}}{\partial z} \tag{35b}$$

where $d/dt = \partial/\partial t + \vec{G} \cdot \vec{\nabla}$ in the latitude-height plane [*Lighthill*, 1978]. Here we have neglected terms involving second-order derivatives of q. One could perform ray-tracing calculations where l and m are integrated following the group velocity from source locations, adjusting the group velocity according to new values of l and m along the paths. *O'Neill and Youngblut* [1982] describe some ray-tracing calculations for Rossby waves. The group velocity is only defined along rays, which may not fill out the space of interest. Ray tracing is not well suited to our application, since we need $\vec{G}$ at all points on the model grid. We seek approximations to (32) and (35) such that $\vec{G}$ can be calculated simultaneously at all grid points, while retaining most of the properties of the exact group velocity.

Most Rossby waves in the middle atmosphere are quasi-stationary. For $\omega \approx 0$, (31*a*) reduces to

$$K^2 = \frac{\bar{q}_y}{\bar{u}} \tag{36}$$

and the group speeds (32) become

$$G_y = \frac{2lk\bar{u}^2}{\bar{q}_y} \tag{37a}$$

$$G_z = \frac{2mk\bar{u}^2}{\bar{q}_y} \frac{f^2}{N^2} \tag{37b}$$

Since the wave forcing is slowly varying, it is reasonable to assume that $\partial l/\partial t$ and $\partial m/\partial t$ are small in (35). If we further assume that l varies more rapidly in latitude than in altitude, while m varies more rapidly in altitude, then (35) may be integrated from reference values (indicated by tilde) to obtain

$$l = \tilde{l} - \int_{\tilde{y}}^{y} \frac{k\, \bar{u}_y}{G_y}\, dy \tag{38a}$$

$$m = \tilde{m} - \int_{\tilde{z}}^{z} \frac{k\, \bar{u}_z}{G_z}\, dz \tag{38b}$$

We choose $l = \tilde{l}$ at $\tilde{\phi}$ for all altitudes and $m = \tilde{m}$ at $\tilde{z}$ for all latitudes.

Finally, reference group speeds are defined:

$$\tilde{G}_y = \frac{2\tilde{l}\tilde{k}\tilde{u}^2}{\tilde{q}_y} \tag{39a}$$

$$\tilde{G}_z = \frac{\tilde{m}}{\tilde{l}} \tilde{G}_y \frac{\tilde{f}^2}{N^2} \tag{39b}$$

From (37) and (39), ratios are formed, yielding formulae which depend only on $\bar{u}$ and ϕ:

$$G_y = \tilde{G}_y \left(\frac{\bar{u}}{\tilde{u}}\right)^2 \frac{\cos\tilde{\phi}}{\cos\phi} \frac{\bar{q}_y}{\tilde{q}_y} \frac{l}{\tilde{l}} \tag{40a}$$

$$G_z = \tilde{G}_z \left(\frac{\bar{u}}{\tilde{u}}\right)^2 \frac{\cos\tilde{\phi}}{\cos\phi} \frac{\bar{q}_y}{\tilde{q}_y} \frac{m}{\tilde{m}} \frac{f^2}{\tilde{f}^2} \tag{40b}$$

At each time, l and m are determined as complete fields by integrating (38), using fields of G_y and G_z from the previous time step, then computing $\vec{G}$ from (40). Thus the group velocity in (28) depends solely on latitude and the varying distribution of model zonal winds. We take N to be constant. Without this separate dependence of l on $\bar{u}_y$ and m on $\bar{u}_z$ provided by (38), $G_z/G_y = (m/l)(f/N)^2$ would have depended only on latitude.

Equations (28), (38), and (40) describe the propagation of Rossby wave activity on a sphere under the assumptions that the background state is slowly varying and that the waves are quasi-stationary and quasi-geostrophic. This WKBJ approach essentially treats a Rossby wave as a continuous field of particles having the local attribute of wave activity. Although some of the simplifying assumptions mentioned earlier may not apply in certain situations, this formulation allows us to make a reasonable estimate of $\vec{\nabla} \cdot \vec{F}$ which varies with $\bar{u}$ in accordance with theory. The method is less valid approaching a low-latitude critical line, ($\bar{u} = 0$ in this case), where $|G_y|$ gets small and $|l|$ gets large.

4. Numerical Algorithm

Equation (28) is solved in the domain 85°S - 85°N, 15-85 km, with a grid spacing of 5° x 1 km, to obtain $A(y, z, t)$. At present, wave generation is represented as a bottom boundary condition on A at 15 km. *Baldwin et al.* [1985], *Shiotani* [1986], and *Randel* [1987] provide useful climatologies of EP fluxes near the tropopause. An estimate of wave activity at 15 km can be obtained by dividing the observed values of F_z by $\tilde{G}_z$. Figure 2 shows the seasonal and latitudinal variation of A at 15 km used in the model runs, an analytic representation of the observed climatology for $k^* = 1$. Values of A are taken to be largest near 55°N, January 1 (~14), with secondary maxima near 55°S, September 1 (~5) and May 1 (~3), in units of 10^6 kg m^{-1} s^{-1}. Note the climatological relative minimum in winter in the southern hemisphere [*Geller and Wu*, 1987].

Specification of wave dissipation is more difficult. Dissipation due to radiative transfer is fairly well understood. Mechanical damping of Rossby wave activity can be caused by turbulence arising from a variety of processes. Although it is possible for breaking gravity waves to amplify a Rossby wave [*Miyahara et al.*, 1986], it seems likely that they would most often have a damping effect. Breaking of the Rossby waves themselves [*McIntyre and Palmer*, 1984] will lead to increased mechanical and radiative damping. Dissipation due to radiative processes and to breaking gravity waves should increase with altitude. Dissipation due to Rossby wave breaking should be largest in the "surf zone," where $\bar{q}_y \leq 0$. Since it is difficult to know the distribution of mechanical damping with certainty, we employ a simple representation of dis-

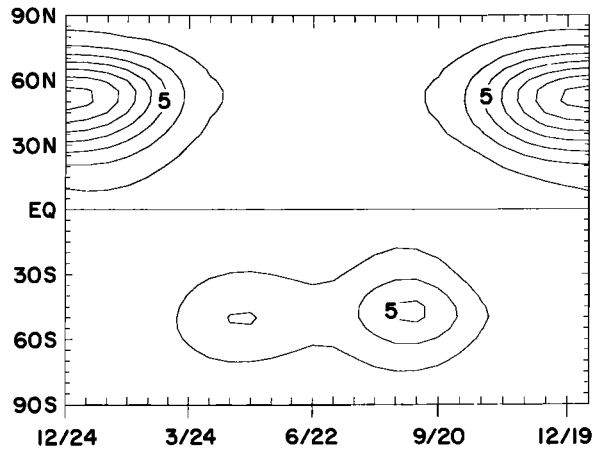

Fig. 2. Time-latitude section of Rossby wave activity at 15 km. This analytic fit to observed climatology is contoured with an interval of 2 x 10^6 kg m^{-1} s^{-1}, beginning at 1 x 10^6 kg $m^{-1}s^{-1}$.

sipation that increases with altitude and with the amount of wave activity: $D = -\alpha(z)\ A$, where

$$\alpha(z) = 0.7 + 0.6 \quad tanh\left[\frac{(z-50)}{15}\right] \tag{41}$$

and z in kilometers gives α in per day. The damping time scale is 9 days at 15 km and 1 day at 60 km.

This linear damping parameterization is compatible with observations, in the sense that wave activity is absorbed where it accumulates. However, Rossby wave breaking is a nonlinear process. Surf zones can be partially reflecting. *McIntyre* [1987] pointed out that nonlinear self-tuning resonant effects can influence where wave activity will accumulate. As theory develops, it may be appropriate to try to model the feedback nature of Rossby wave absorption in the presence of a surf zone.

To establish the group velocity, (38) and (40) require reference values. Reference locations are chosen to be $\tilde{z}$ = 15 km and $\tilde{\phi} = 55°$ in each hemisphere. Reference group speeds are $\tilde{G}_y$ = 3.5 m s^{-1} and $\tilde{G}_z$ = 0.027 m s^{-1}, which were estimated from (32) and observed length scales [*Hitchman et al.*, 1987]. We study quasi-stationary planetary wave one: $\omega = 0$ and $k^* = 1$, which defines $\tilde{k} = k^*/(a\ cos\ \tilde{\phi})$. Quasi-stationary $k^* = 1$ is observed to be the dominant planetary Rossby wave in the middle atmosphere, although there are times when a traveling $k^* = 2$ dominates in the southern hemisphere [*Randel*, 1987; *Geller and Wu*, 1987]. The value of m is found by integrating (38*b*) upward from $\tilde{z}$, where $\tilde{m} = 2\pi/(30$ km). Here l is found separately in each hemisphere by integrating poleward and equatorward from $\tilde{\phi}$ in each hemisphere, where $\tilde{l} = 2\pi$ /(180° latitude). In the southern hemisphere $\tilde{l}$ is positive and in the northern hemisphere $\tilde{l}$ is negative. Reasonable limits on m are set to be $2\pi/(30$ km) and $2\pi/(200$ km). Limits on l are $2\pi/(30°)$ and $2\pi/(180°)$. In (40), $\tilde{q}_y = (2\Omega/a)\ cos\ \tilde{\phi}$, $\tilde{f} = 2\Omega\ sin\ \tilde{\phi}$, and $\tilde{u}$ = 20 m s^{-1} (corresponding to $\bar{u}$ at $\tilde{\phi}$, $\tilde{z}$). In the algorithm, $\tilde{G} = 0$, if $\bar{u} < 0$. Here $\bar{q}_y$ is constrained to be at least as large as $\tilde{q}_y/2$ to avoid wave activity growth by barotropic instability.

As with the temperature and constituent equations, (28) is solved with an implicit time integration scheme, using an alternating direction method. Equations (38) and (40) are iterated 10 times for each 15-day time step with fixed $\bar{u}$. With the 15-day time step, it is possible to multiply the envelope in Figure 2 by a random number at each time, yielding a "stochastic" Rossby wave forcing pattern that somewhat approximates natural Rossby wave variability. Only results from the "continuous" forcing will be presented. The values of A shown in Figure 2 constitute the bottom boundary condition. The upper boundary condition is $A = 0$, while $\partial A/\partial y = 0$ at the poles. The conditions $A = 0$ and $\vec{\nabla} \cdot \vec{F} = 0$ were also tried at the poles. Nevertheless, all methods yielded a region where $\vec{\nabla} \cdot \vec{F} > 0$ near the the poles. The cause of this may be that we require $A \geq 0$ at all points, and errors in finite differencing introduce extra wave activity at the pole when the group velocity is equatorward. In (9) and (23) we also set $\vec{\nabla} \cdot \vec{F} = 0$ if it exceeds zero.

Background values of K_{yy} are set to be 3 x 10^5 m^2 s^{-1}, which is representative of typical low values derived from observations during relatively undisturbed times [*Newman et al.*, 1986, 1988; *Lyjak*, 1987]. The present parameterization of the variable portion of K_{yy} is our best estimate of mixing by quasi-stationary planetary scale Rossby wave one excited in the mid-latitude troposphere. The background nonzero K_{yy} is intended to encompass mixing processes arising from other phenomena, such as inertio-gravity waves and traveling Rossby waves.

Before showing the structure of the wave activity, it is necessary to point out that a single coherent Rossby wave may fill a space in which the mean flow varies considerably. i.e., the WKBJ approximation may not be valid. It has been found in other studies, however, that WKBJ group velocities are reasonable to use in this situation, provided the background flow values are smoothed considerably. This is in keeping with the idea that large coherent waves "feel" a spatially averaged background state. For example, in calculating teleseismic tsunami ray paths, *Woods and Okal* [1987] smoothed group velocities in accordance with a typical wavelength of 300 km. In comparing observed Kelvin waves with the two-dimensional WKBJ dispersion relation governing internal gravity waves, *Hitchman and Leovy* [1988] found good agreement for relatively short waves and an improved agreement for tall waves when a vertical mean $\bar{u}$ was used instead of the local $\bar{u}$ in the dispersion relation. Presently, we smooth $\bar{u}$ with a $\frac{1}{4} - \frac{1}{2} - \frac{1}{4}$ filter, so that it varies more slowly than wave phase in mid-latitudes, prior to use in (38) and (40).

Figure 3 shows latitude-height sections of temperature and zonal wind (unsmoothed) on December 29 after 4.5 years of model integration. Below 12 km we use fixed monthly mean temperatures from the climatology compiled by *Randel* [1987]. Use of the tropospheric temperature climatology slightly increased lower stratospheric winds, facilitating the upward transport of wave activity. The temperatures and zonal winds in Figure 3 are similar to observed solstice conditions [*Boville and Randel*, 1986]. Zonal winds are smoothed in latitude and height for use in solving (28).

From (38) one expects that m will decrease upward into the winter westerlies, then increase above the jet maximum, and that $|l|$ will increase equatorward toward

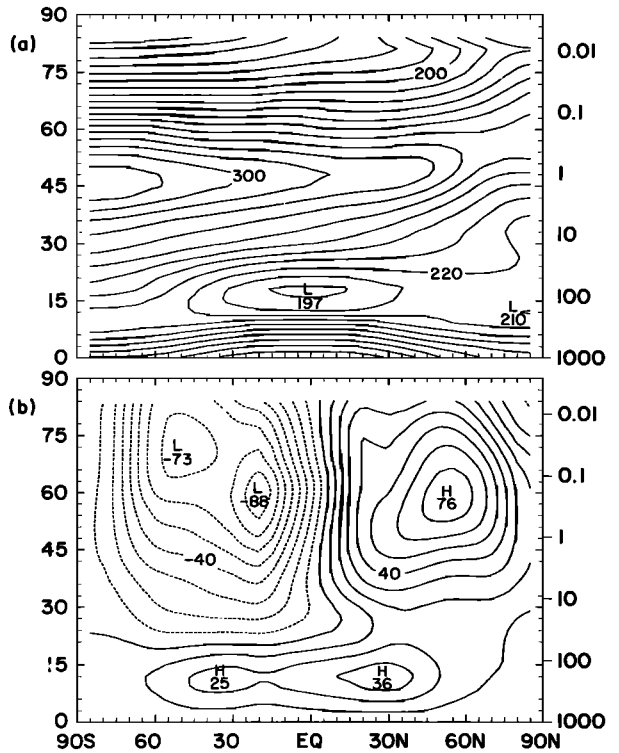

Fig. 3. Latitude-height sections on December 29 after 4.5 years of model integration of zonal mean (*a*) temperature, contour interval 10 K, and (*b*) zonal wind, contour interval 10 m s^{-1}.

the zero wind line. This is verified in Figure 4. The meridional wavelength is smallest at low latitudes (Figure 4*a*). The vertical wavelength is largest in the westerly jet (Figure 4*b*). This may be relevant to the observation that Rossby waves in the middle atmosphere generally tilt less with height than those in the troposphere. Although l is solved for separately in the two hemispheres, l is smoothly negative in the equatorial lower mesosphere. In (40) this allows for cross-equatorial propagation in cases where there are equatorial mesospheric westerlies (not shown). It can be seen in Figure 4 that the WKBJ relations (38) give a more rapid variation of wavelengths than is physically reasonable, even with highly smoothed winds, necessitating the use of reasonable limits on wave scales.

Sections of G_y and G_z are shown in Figure 5. Here $|\vec{G}|$ tends to increase toward the pole because of the geometrical convergence factors embodied in $k \propto (\cos\phi)^{-1}$ and $\bar{q}_y \propto \cos\phi$ in (37). The $|\vec{G}|$ also tends to be large in the westerly jet and decreases toward the critical line, this effect being represented by $\bar{u}^2$ in (37). Typical winter values are $G_y = 20^\circ$ day^{-1} toward the equator and $G_z = 4$ km day^{-1} upward.

Rossby wave activity wells up out of the troposphere, filling out the westerlies, being absorbed as it propagates (Figure 6*a*). The EP flux arrows turn strongly equatorward below the jet at this time (Figure 6*b*). This pattern is similar to that for certain weeks during the Limb Infrared Monitor of the Stratosphere (LIMS) data record. It is also similar to results obtained by *Robinson* [1986], who diagnosed a linear wave model for zonal wave two using the group velocity concept. The strongest absorption occurred in the mid-latitude middle stratosphere at this time, with a maximum easterly torque of 7 m s^{-1} day^{-1} (Figure 6*b*). Irreversible mixing is strongest where waves are being absorbed. A typical magnitude for K_{yy} in the region of wave absorption is 2 x 10^6 m^2 s^{-1} (Figure 6*c*).

The variation in distributions of K_{yy} with season and with method of calculation is rather large. *Lyjak* [1987] calculated parcel dispersion using a Lagrangian advection algorithm with LIMS three-dimensional winds and found K_{yy} to be largest in a broad region centered near 5 mbar and 30° in the winter hemisphere. *Newman et al.* [1986, 1988] used 4 years of National Meteorological Center data, together with (21), and found largest K_{yy} values at a higher altitude, near 1 mbar. Negative regions can occur with both of these methods. *Plumb and Mahlman* [1987] used output from the SKYHI general circulation model and found that the largest values occurred at the model zero wind line. We feel that our results are compatible with previous estimates based on observations. LIMS observations show that wave absorption is largest about 20° poleward of the zero wind line [*Hitchman et al.*, 1987]. The contention that K_{yy} is largest where wave absorption is largest is compatible with the SKYHI results if waves in the SKYHI model are absorbed most strongly near the model zero wind line.

Distributions of $\vec{\nabla} \cdot \vec{F}$ and K_{yy} are quite sensitive to the distribution of $\bar{u}$. *Robinson* [1986], with insight gained from control through the invertibility principle, determined that in his linear wave model, small changes in the zonal wind field induced by the isentropic rearrangement of potential vorticity resulted in significant changes

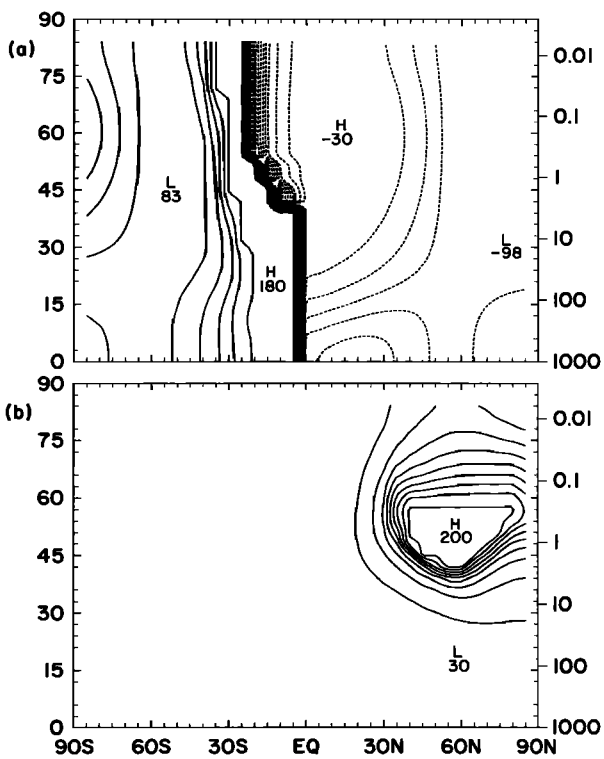

Fig. 4. As in Figure 3 on December 29 for $k^* = 1$, except for (*a*) meridional wavelength, $2\pi/l$, contour interval 20° latitude, and (*b*) vertical wavelength, $2\pi/m$, contour interval 20 km (see text).

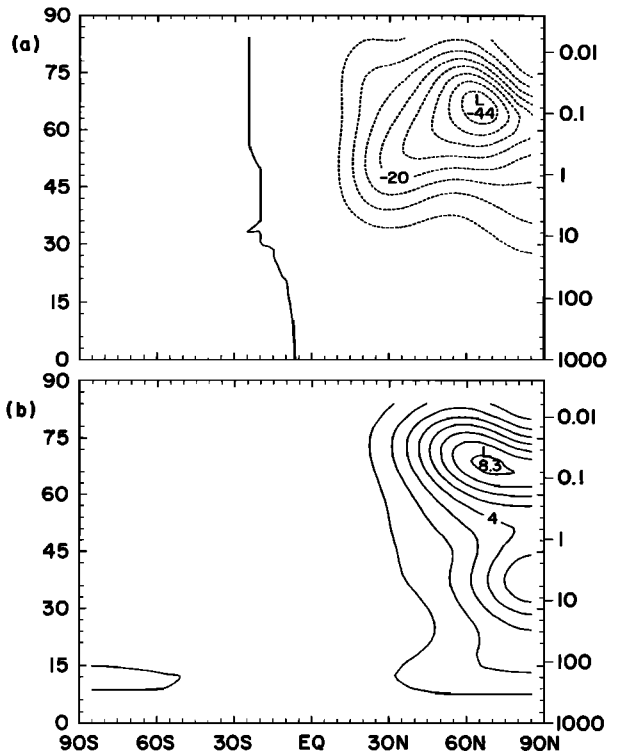

Fig. 5. As in Figure 3 on December 29 for $k^* = 1$, except for (*a*) meridional group speed, contour interval 5° latitude day^{-1} and (*b*) vertical group speed, contour interval 1 km day^{-1}.

in the distribution of wave activity. We are in the process of fully exploring the sensitivity of our parameterization. The response is linear in tropospheric forcing, is not very sensitive to $\alpha(z)$, but can vary considerably with changes in $\bar{u}(y, z)$. The example in Figure 7 illustrates the sensitivity to $\bar{u}$. On February 27, during the fifth year of model integration, the westerly jet was displaced poleward relative to that on December 29 (compare Figures 7*a* and 3*a*). Wave activity penetrated to higher altitudes in February, being absorbed primarily in the lower mesosphere (Figure 7*b*). The elevated region of large K_{yy} (Figure 7*c*) is very similar to the results of *Newman et al.* [1988].

In Figures 4-7 we show values below 15 km altitude, although they are not used in the present model. Currently, the tropospheric stream function is fixed. Thus the troposphere is not interactive. This strongly affects results near the tropopause. In the real troposphere many processes contribute to equatorial upwelling and polar sinking, including Rossby wave driving. A future version of the model will allow a portion of the tropospheric circulation to vary consistently with Rossby wave driving in the middle atmosphere.

5. Influence on Mean Flow and Constituents

We now compare results for two model runs with identical physics, except that in run 1 the Rossby wave parameterization was turned off. Both runs include the constant background value of K_{yy} and the interactive gravity wave parameterization. Run 2 includes F_R, which can alter $(\bar{v}^*, \bar{w}^*)$, hence $\bar{T}$ and $\bar{u}$, and includes the variable part of K_{yy}, which leads to greater mixing. Figure 8*a* shows the stream function on December 29 for run 2. One can see the mesospheric summer to winter flow driven by gravity waves [cf. *Brasseur and Hitchman* 1987] as well as the stratospheric low-latitude ascent, poleward flow, and descent over the poles. In the current model the lower stratospheric circulation is controlled primarily by the specified tropospheric stream function. The difference in χ between the two runs (run 2 − run 1) is shown in Figure 8*b*. Rossby wave absorption causes an easterly torque, which can be balanced by a poleward flow of high angular momentum air from low latitudes, far from the rotation axis. This pattern is essentially that obtainable from $-f\bar{v}^* = F_R$ and (3), modified by concomitant changes in heating rates due to dynamically

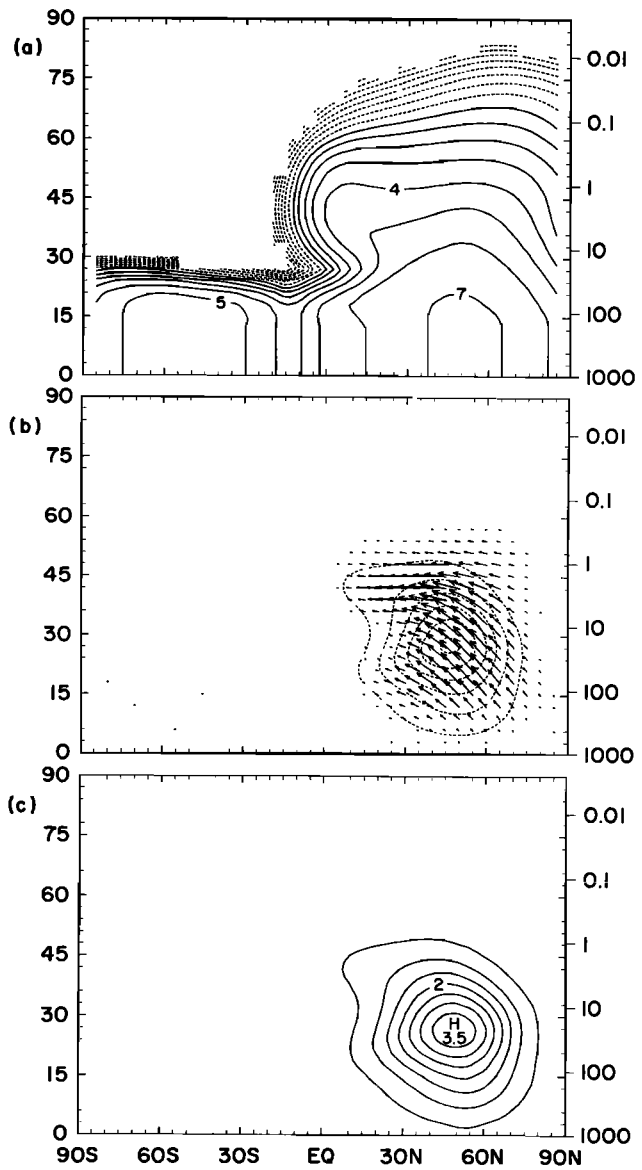

Fig. 6. As in Figure 3 on December 29 for $k^* = 1$, except for (*a*) $\log_{10}$ of Rossby wave activity, contour interval 1.0, (*b*) EP fluxes and body force per unit mass, contour interval 1 m s^{-1} day^{-1}, and (*c*) meridional eddy diffusivity, contour interval 5 x 10^5 m^2 s^{-1}. The background value is 3 x 10^5 m^2 s^{-1}. In Figure 6*b* the components plotted are F_y/ρ_o and 143 x F_z/ρ_o. The maximum vector length is 5.1 x 10^8 kg s^{-2}. Values of A below 15 km are set to the values at 15 km.

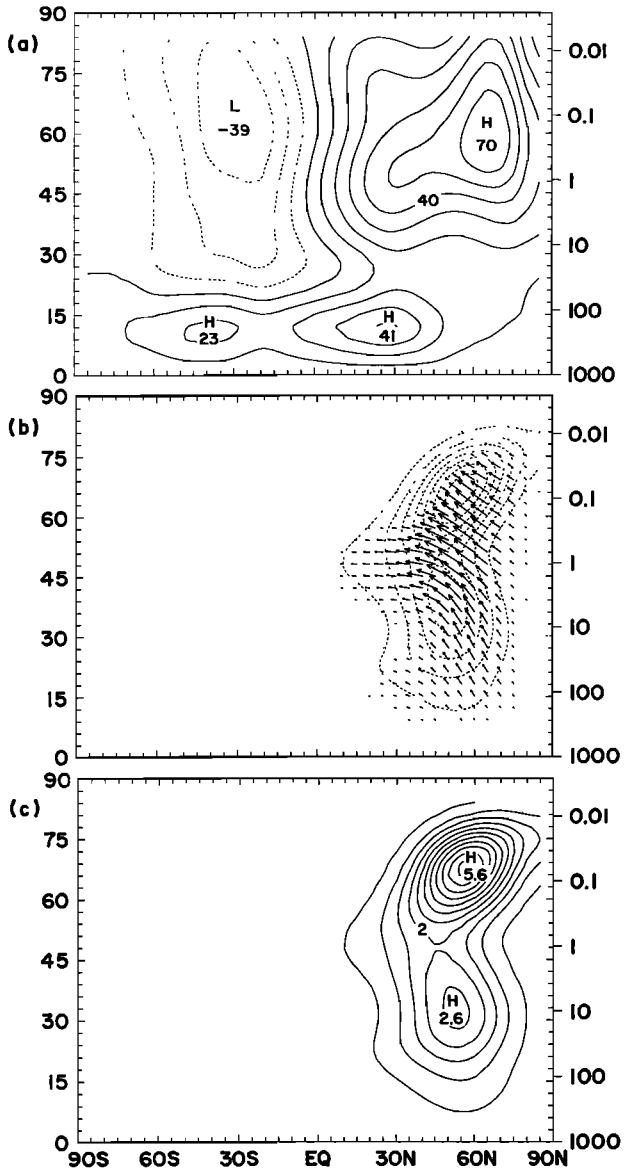

Fig. 7. Latitude-height sections on February 27 for $k^* = 1$, after 4.5 years of model integration of zonal mean (*a*) zonal wind, contour interval 10 m s^{-1}, (*b*) EP fluxes and body force per unit mass, contour interval 1 m s^{-1} day^{-1}, and (*c*) meridional eddy diffusivity, contour interval 5 x 10^5 m^2 s^{-1}. The background value is 3 x 10^5 m^2 s^{-1}. In Figure 7*b* the components plotted are F_y/ρ_o and 143 x F_z/ρ_o. The maximum vector length is 8.3 x 10^8 kg s^{-2}.

induced temperature and ozone changes. An unfortunate consequence of the fixed tropospheric streamfunction is that the perturbed flow has a thin return stream near 15 km (Figure 8*b*).

Rossby wave absorption causes a warming of the polar lower stratosphere through induced descent (~7 K in this case, not shown). As one may infer from (4), the winter westerlies are reduced at high latitudes in run 2 relative to run 1. This alters the breaking levels for gravity waves, causing changes in F_g and K_{zz}, which, in turn, alter mesospheric tracer transport. The rich spectrum of feedbacks in the model will be described more completely elsewhere.

Figure 9*a* shows the distribution of model N_2O for run 2 on February 27. N_2O is produced by life processes in the troposphere and is photodissociated at upper levels. In the lower stratosphere it is a relatively conserved species. As with the observed distribution, N_2O concentrations decrease upward and away from the equator. This is as expected for a tracer being advected by circulations similar to that in Figure 8*a*. N_2O concentrations are relatively low near 50 km over the north pole. This is due to the gravity wave driven summer to winter circulation, which advects low values of N_2O down over the winter pole. This descending region of low N_2O values is "clipped" by enhanced meridional mixing associated with large K_{yy} values in the winter mid latitudes (Figures 6*c*, 7*c*). Figure 9*c* shows the percent difference in N_2O concentration between runs 1 and 2 (run 2 − run 1). As found by *Jackman et al.* [1988], locally enhanced meridional mixing causes a downgradient flux. N_2O concentrations are more than doubled near 10 mbar over the winter pole relative to run 1. During the southern spring the Rossby wave parameterization caused enhanced N_2O values over the south pole, which were subsequently advected to higher altitudes, yielding larger N_2O concentrations in the south polar mesosphere relative to run 1.

Figure 10*a* shows the distribution of model ozone for run 2 on December 29. Ozone mixing ratios (not shown) decrease monotonically away from the tropical production region. Ozone concentration is useful for showing the relative contribution to total column amounts by each layer. Above 20 km a higher concentration of ozone

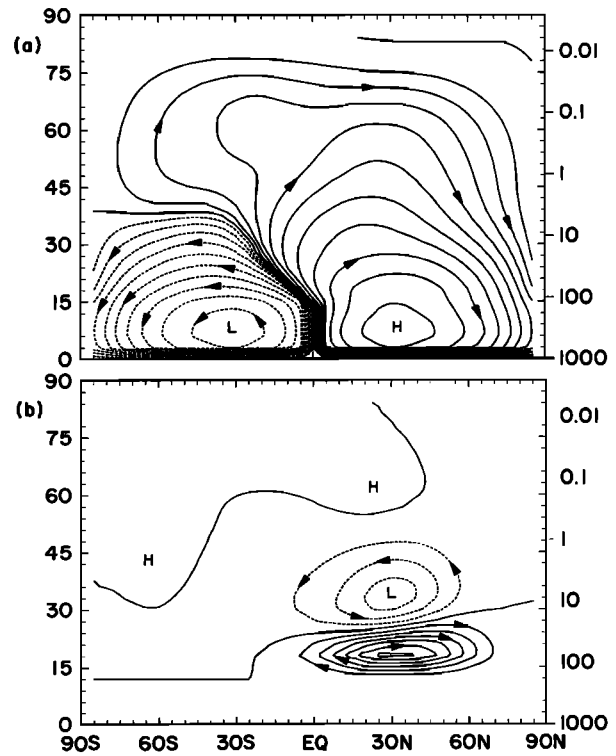

Fig. 8. As in Figure 3 on December 29, except for (*a*) $\log_{10}$ of the residual stream function for run 2 (see text) and (*b*) the difference in stream function for runs 1 and 2 (run 2 − run 1), contour interval 5 m^2 s^{-1}.

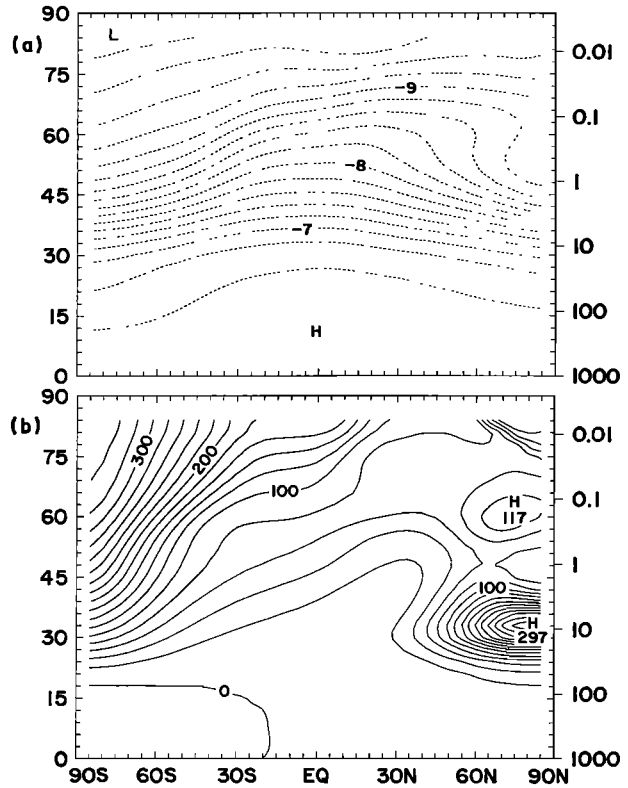

Fig. 9. As in Figure 7 on February 27, except for (*a*) $\log_{10}$ of nitrous oxide mixing ratio, contour interval 0.2, and (*b*) the percent difference in N_2O, contour interval 20%.

is found in the tropics, while below 20 km a higher concentration is found in the polar reservoirs, a product of transport processes. Figure 10*b* shows the percent changes in ozone concentration due to the Rossby wave parameterization. Again, meridional gradients are reduced where K_{yy} is enhanced. With more mixing (Figure 6*c*), polar ozone is increased above ~20 km and reduced below that level (Figure 10*b*). Rossby wave absorption causes enhanced advection of ozone poleward and downward (Figure 8*b*). The spurious return flow near 100 mbar contributes to ozone loss near 15 km. Because of higher ozone concentrations at lower altitudes, the column ozone amount at high latitudes actually decreased with increased Rossby wave absorption. This result has made it clear that (1) the variation of K_{yy} near the tropopause must be treated carefully, and (2) the tropospheric circulation must be allowed to change along with Rossby wave absorption in the middle atmosphere.

6. Conclusions

By adding a single equation for conservation of Rossby wave activity to a system of zonal mean equations, one may close the system for Rossby wave driving and meridional eddy fluxes in a manner that varies self-consistently with model zonal winds. While simple to calculate, the group velocity parameterization is fairly flexible in that varying degrees of poleward or equatorward refraction can occur. Although there are several simplifying assumptions underlying the group velocity representation, we believe that the feedback capability of this method may make it preferable to climatological specifications for many applications. The differences between Figures 6 and 7 illustrate that with very similar wave generation and damping for the two times, wave driving can vary considerably with the changing zonal flow.

A hypothesis underlying the applicability of wave activity conservation to tracer mixing is that the same physics leading to wave absorption also lead to irreversible mixing. The method provides a means of estimating a spatially varying K_{yy} that can be applied to other tracers, provided the photochemical time scale is known for that tracer. At present, we are applying the same distribution of K_{yy} to all tracers. *Smith et al.* [1988] have obtained some interesting results for the photochemical transport of certain observed tracers. With climatological values of the upward flux of Rossby wave activity near the tropopause, we obtain typical winter stratospheric values of ~2 x 10^6 m^2 s^{-1}. Given that the model gravity wave driven meridional circulation causes realistically strong downward tracer advection over the winter pole, substantial meridional mixing is required to flatten meridional gradients in the stratosphere to observed slopes.

A useful application of this parameterization is in providing a feedback for planetary wave effects in scenario calculations. Changes in radiatively active species can change the zonal wind structure, which affects the distribution of wave-driven advection and mixing of these species. Since the physics of wave propagation are reasonably represented, the model could be used to study past and future atmospheric structure. *Brasseur and Hitchman* [1988] studied the changes in the model due to increased chlorofluorocarbons and carbon dioxide. They found that the latitudinal variation in column ozone changes due to

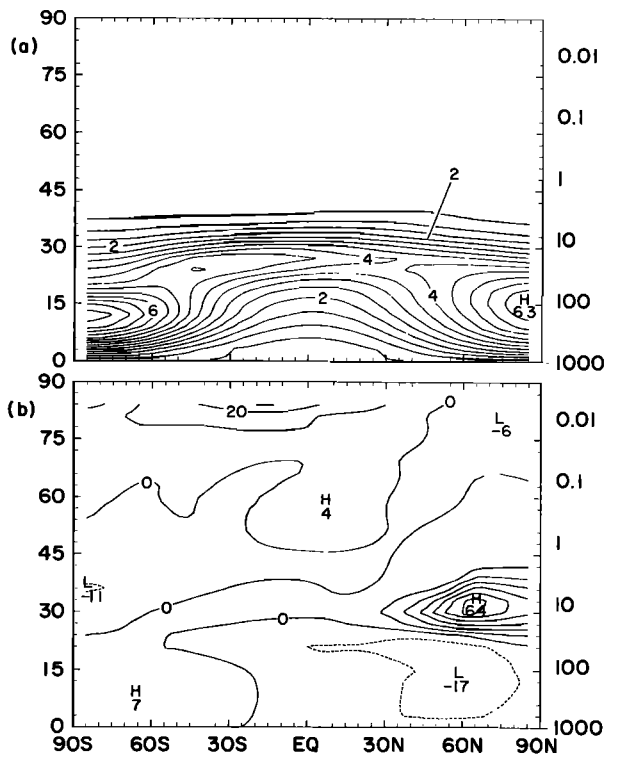

Fig. 10. As in Figure 3 on December 29, except for (*a*) ozone concentration, contour interval 5 x 10^{11} molecules cm^{-3}, and (*b*) percent difference in ozone, contour interval 10%.

these anthropogenic trace gases depended on whether the Rossby wave parameterization was included. Interesting results for very large imposed ozone depletions in the NCAR Community Climate Model are reported by *Kiehl and Boville* [1988] for perpetual January conditions. We hope that application of the concept of Rossby wave activity will allow two-dimensional modelers to carry out multiyear integrations in investigating scenarios where changes in the mean flow and wave driving may be substantial.

NOTATION

$\overline{(\ )}$, $(\ )'$	Eulerian zonal mean and deviation.
$(\ )$	reference value.
A	Rossby wave activity.
a	radius of the Earth.
C_F	forcing term in stream function equation.
c, c_r, c_i	zonal trace speed, real, and imaginary parts.
F_R, F_g	body force per unit mass due to Rossby and gravity waves.
F_y, F_z	components of the EP flux.
D	dissipation of wave activity.
D_θ, D_μ	flux convergence terms for entropy and tracer equations.
f	Coriolis parameter.
G_y, G_z	meridional and vertical group speeds.
H	scale height.
K_{yy}, K_{zz}	meridional and vertical eddy mixing coefficients.
k, l, m	zonal, meridional, and vertical wave numbers.
k^*	nondimensional zonal wave number.
N	buoyancy frequency.
n	meridional index of Legendre polynomial.
Q	heating rate for potential temperature.
q	quasi-geostrophic potential vorticity.
q_y	northward gradient of basic state potential vorticity.
R	gas constant for dry air.
S	source term.
s	zonal index of Legendre polynomial.
T	temperature.
u, v, w	zonal, meridional, and vertical wind components.
$\overline{v}^*$, $\overline{w}^*$	Eulerian mean residual circulation.
α	damping rate.
β	northward gradient of planetary vorticity.
γ	modified Coriolis parameter.
ζ'	upward parcel displacement.
η	absolute vorticity.
η'	northward parcel displacement.
θ	potential temperature, wave phase.
λ	longitude.
μ	tracer mixing ratio.
ρ_o	basic state density.
τ_m, τ_r	mechanical and photochemical damping time scales.
τ_a, τ_g	advective and wave growth time scales.
ϕ	latitude.
χ	residual mean meridional stream function.
Ω	angular frequency of Earth's rotation.
ω	wave frequency.

Acknowledgments. We would like to thank Donal O'Sullivan for many useful discussions of the group velocity parameterization. We are grateful to Bill Randel for providing the 8-year NMC tropospheric temperature climatology. We would also like to thank Byron Boville, Rolando Garcia, John Gille, Peter Haynes, Walter Robinson, Murry Salby, and Anne Smith for useful conversations. Paul Newman and Hans-Rainer Schneider gave helpful reviews. This work was supported by NASA's Upper Atmosphere Research Program, under grant WA-16215. G.B. is supported by the Belgian National Fund for Scientific Research. The National Center for Atmospheric Research is sponsored by the National Science Foundation.

REFERENCES

Andrews, D. G., On the interpretation of the Eliassen-Palm flux divergence, *Q. J. R. Meteorol. Soc., 113*, 323-338, 1987.

Baldwin, M. P., H. J. Edmon, Jr. and J. R. Holton, A diagnostic study of eddy-mean flow interactions during FGGE SOP-1, *J. Atmos. Sci., 42*, 1838-1845, 1985.

Boville, B. A., and W. J. Randel, Observations and simulation of the variability of the stratosphere and troposphere in January, *J. Atmos. Sci., 43*, 3015-3034, 1986.

Brasseur, G., and M. H. Hitchman, The effect of breaking gravity waves on the distribution of trace species in the middle atmosphere, in *Transport Processes in the Middle Atmosphere*, pp. 215-227, D. Reidel, Hingham, Mass., 1987.

Brasseur, G., and M. H. Hitchman, Stratospheric response to trace gas perturbations: Changes in ozone and temperature distributions, *Science, 240*, 634-637, 1988.

Butchart, N., S. A. Clough, T. N. Palmer, and P. J. Trevelyan, Simulation of an observed stratospheric warming with quasi-geostrophic refractive index as a model diagnostic, *Q. J. R. Meteorol. Soc., 108*, 475-502, 1982.

Carnahan B., H. A. Luther, and J. O. Wilkes, *Applied Numerical Methods*, chap. 7, John Wiley, New York, 1969.

Coy, L., and D. C. Fritts, Gravity wave heat fluxes: A Lagrangian approach, *J. Atmos. Sci.*, in press, 1988.

Edmon, H. J., B. J. Hoskins, and M. E. McIntyre, Eliassen-Palm cross sections for the troposphere, *J. Atmos. Sci., 37*, 2600-2616, 1980.

Garcia, R. R., and S. Solomon, A numerical model of the zonally averaged dynamical and chemical structure of the middle atmosphere, *J. Geophys. Res., 88*, 1379-1400, 1983.

Garcia, R. R., and S. Solomon, The effect of breaking gravity waves on the dynamics and chemical composition of the mesosphere and lower thermosphere, *J. Geophys. Res., 90*, 3850-3868, 1985.

Geller, M. A., and M. F. Wu, Troposphere-stratosphere general circulation statistics, in *Transport Processes in the Middle Atmosphere*, pp. 3-17, D. Reidel, Hingham, Mass., 1987.

Gray, L. G., and J. A. Pyle, Two-dimensional studies of equatorial dynamics and tracer distributions, *Q. J. R. Meteorol. Soc., 113*, 635-651, 1987.

Haurwitz, B., The motion of atmospheric disturbances on the spherical earth, *J. Mar. Res., 3*, 254-267, 1940.

Hitchman, M. H., and C. B. Leovy, Estimation of the Kelvin wave contribution to the semiannual oscillation, *J. Atmos. Sci.*, in press, 1988.

Hitchman, M. H., C. B. Leovy, J. C. Gille, and P. L. Bailey, Quasi-stationary zonally asymmetric circulations in the equatorial lower mesosphere, *J. Atmos. Sci., 44*, 2219-2236, 1987.

Holton, J. R., Wave propagation and transport in the middle atmosphere, *Philos. Trans. R. Soc. London, Ser. A., 296*, 73-85, 1980.

Holton, J. R., The role of gravity wave induced drag and diffusion in the momentum budget of the mesosphere, *J. Atmos. Sci., 39*, 791-799, 1982.

Hoskins, B. J., A. J. Simmons, and D. G. Andrews, Energy dispersion in a barotropic atmosphere, *Q. J. R. Meteorol. Soc., 103*, 553-567, 1977.

Jackman, C. H., P. A. Newman, P. D. Guthrie, and M. R. Schoeberl, Effect of self-consistent horizontal diffusion coefficients on two-dimensional N_2O model distributions, *J. Geophys. Res.*, in press, 1988.

Kida, H., General circulation of air parcels and transport characteristics derived from a hemispheric GCM, 1, A determination of advective mass flow in the lower stratosphere, *J. Meteorol. Soc. Jpn., 61*, 171-186, 1983.

Kiehl, J. T., and B. A. Boville, The radiative-dynamical response of a stratospheric-tropospheric general circulation model to changes in ozone, *J. Atmos. Sci.*, in press, 1988.

Lighthill, J., *Waves in Fluids*, p. 327, Cambridge University Press, New York, 1978.

Lindzen, R. S., Turbulence and stress due to gravity wave and tidal breakdown, *J. Geophys. Res.*, *86*, 9707-9714, 1981.

Lyjak, L. V., Diffusion coefficients calculated from satellite data, in *Transport Processes in the Middle Atmosphere*, pp. 343-352, D. Reidel, Hingham, Mass., 1987.

McIntyre, M. E., Dynamics and tracer transport in the middle atmosphere: An overview of some recent developments, in *Transport Processes in the Middle Atmosphere*, pp. 267-296, D. Reidel, Hingham, Mass., 1987.

McIntyre, M. E., and T. N. Palmer, The "surf-zone" in the stratosphere, *J. Atmos. Terr. Phys.*, *46*, 825-849, 1984.

Miyahara, S., Y. Hayashi, and J. D. Mahlman, Interactions between gravity waves and planetary-scale flow simulated by the GFDL "SKYHI" general circulation model, *J. Atmos. Sci.*, *43*, 1844-1861, 1986.

Newman, P. A., M. R. Schoeberl, and R. A. Plumb, Horisontal mixing coefficients for two-dimensional chemical models calculated from National Meteorological Center data, *J. Geophys. Res.*, *91*, 7919-7924, 1986.

Newman, P. A., M. R. Schoeberl, R. A. Plumb, and J. E. Rosenfield, Mixing rates calculated from potential vorticity, *J. Geophys. Res.*, in press, 1988.

O'Neill, A., and C. E. Youngblut, Stratospheric warmings diagnosed using the transformed Eulerian mean equations and the effect of the mean state on wave propagation, *J. Atmos. Sci.*, *39*, 1370-1386, 1982.

Plumb, R. A., and J. D. Mahlman, The zonally averaged transport characteristics of the GFDL general circulation/transport model, *J. Atmos. Sci.*, *44*, 298-327, 1987.

Randel, W. J., Global atmospheric circulation statistics, 1000-1 mb, *NCAR Tech. Note 295*, Natl. Cent. for Atmos. Res., Boulder, Colo., 1987.

Robinson, W., The behavior of planetary wave 2 in preconditioned zonal flows, *J. Atmos. Sci.*, *43*, 3109-3121, 1986.

Schoeberl, M. R., and M. A. Geller, A calculation of the structure of stationary planetary waves in winter, *J. Atmos. Sci.*, *34*, 1235-1255, 1977.

Schoeberl, M. R., and D. F. Strobel, The zonally averaged circulation of the middle atmosphere, *J. Atmos. Sci.*, *35*, 577-591, 1978.

Shiotani, M., Planetary wave activity in the troposphere and stratosphere during the northern hemisphere winter, *J. Atmos. Sci.*, *43*, 3200-3209, 1986.

Smith, A. K., L. V. Lyjak, and J. C. Gille, The eddy transport of nonconserved trace species derived from satellite data, *J. Geophys. Res.*, in press, 1988.

Tung, K. K., A coupled model of zonally averaged dynamics, radiation, and chemistry, in *Transport Processes in the Middle Atmosphere*, pp. 183-198, D. Reidel, Hingham, Mass., 1987.

Wallace, J. M., Trajectory slopes, countergradient heat fluxes and mixing by lower stratospheric waves, *J. Atmos. Sci.*, *35*, 554-558, 1978.

Woods, M. T., and E. A. Okal, Effect of variable bathymetry on the amplitude of teleseismic tsunamis: A ray-tracing experiment, *Geophys. Res. Lett.*, *14*, 765-768, 1987.

G. Brasseur, Institut D'Aeronomie Spatiale, 3 Avenue Circulaire, Brussels 1180, Belgium.

M. H. Hitchman, Department of Meteorology, University of Wisconsin-Madison, Madison, WI 53706.

(Received December 7, 1987;
revised February 16, 1988;
accepted February 16, 1988.)